Negative index metamaterial through multi-wave interactions: numerical proof of the concept of low-frequency Lamb-wave multiplexing

Martin Lott[1], Philippe Roux[1], Matthieu Rupin[2], Daniel Colquitt[3] and Andrea Colombi[4]

[1]University Grenoble Alpes, University Savoie Mont Blanc, CNRS, IRD, IFSTTAR, ISTerre, 38000 Grenoble, France.
[2]Hap2U, CIME Nanotech, Grenoble, France
[3]Department of Mathematical Sciences, University of Liverpool, Liverpool, L69 7ZL, UK
[4]Department of Civil, Environmental and Geomatic Engineering, Institute of Structural Engineering, Swiss Federal Institute of Technology, Zurich, Switzerland.

Abstract

We study numerically the potential of a multimodal elastic metamaterial to filter and guide Lamb waves in a plate. Using a sub-wavelength array of elongated beams attached to the plate, and combining the coupling effects of the longitudinal and flexural motion of these resonators, we create narrow transmission bands at the flexural resonances of the beams inside the wide frequency bandgap induced by their longitudinal resonance. The diameter of the beams becomes the tuning parameter for selection of the flexural leakage frequency, without affecting the main bandgap. Finally, by combination of the monopolar and dipolar scattering effects associated with the coupled beam and plate system, we create a frequency-based multiplexer waveguide in a locally resonant metamaterial.

Introduction

Recent advances in elastic metamaterial design have demonstrated the potential of such metamaterials for the control of wave flow through tuning their mechanical properties at the sub-wavelength scale. Many devices have been successfully tested so far, like lenses [1, 2, 3] or waveguides [4, 5, 6], which have all been based on different physical principles. For example, focusing across a slab can be achieved due to anisotropy and spectral overlap [7, 8, 9], gradient index lenses [3], and coupled resonant modes [10, 11]. Similarly, wave-guides in metamaterials can be obtained through topological insulation techniques [12] and nonlinear harmonics migration [13], and even simpler, with defect-like lines [14, 15].

In the following, we present a combination of these physical principles to build a particular elastic waveguide; a multiplexer that can spatially filter an incident plane wave into different point-like sources for the A_0 Lamb mode. Such multiplexing is made possible through the overlap of two resonant modes of the unit cell of our metamaterial. The metamaterial is constituted of elongated beams attached to a plate, which can couple with the first antisymmetric A_0 Lamb mode with two types of motions, one longitudinal and one flexural.

We start by recalling previous results for this metasurface made of closely spaced beams. It was first introduced in 2014 by [16], and it has been studied in many ways since: e.g., with numerical simulations, analytical treatments, and experimental observations [17, 18, 19, 3]. The dominant effect, which is not connected to the spatial configuration of the beams (i.e., ordered vs disordered), is linked to the low quality factor longitudinal resonance of the beams, which creates wide bandgaps and exotic dispersion curves for the first antisymmetric A_0 Lamb mode propagation. On top of this, if the plate is thin enough, the flexural resonance create narrow frequency band perturbation, affecting both S0 and A0 Lamb mode. Colquitt et al. [19] proposed an analytical formula for the dispersion curve calculation of the plate + beam system. In this analysis, the wave propagation inside the metamaterial is governed by a set of equations, involving the two Lamb modes S0 and A0 in the plate and the two resonances of the beams (longitudinal and flexural). The longitudinal resonance of the beams only interacts with the A0 Lamb mode, the flexural resonance interacts both with A0 and S0 through coupling terms (Eq. 2.1a-c in [19]) The dispersion equation is obtained in a closed form but no effective parameters such as the Young modulus or the Bulk density can be expressed. On the other hand, the flexibility of the model makes it possible to consider or eliminate the flexural motion of the resonators that is essential in the proposed multiplexing design. Figure 1 shows dispersion curves computed from Colquitt et al. [19], with or without the flexural resonance effects (panels (a) and (b)), considering the unit cell parameters defined in Fig. 1c. The A0 and S0 free plate response (without the beams) are depicted in gray in Fig. 1a. The bandgap induced by the compressional motion is highlighted by the red background color and the blue curve (Fig 1b) includes the beam flexural resonance effects. Figure 1b highlights that the flexural resonances may have different effects according to the frequency of the plate waves in the metamaterial region. In the passband, they interact with the A0 wave but the coupling term is weak and the A0 wave dominates. In the bandgap, where A_0 mode propagation is forbidden, the flexural resonances generated narrow transmission bands, which creates energy leakage from outside to inside the metamaterial (and vice-versa).

In the following, we show that the start of the main bandgap is underpinned solely by the beam length, and the frequency position of the narrow leakage inside the bandgap due to the beam flexural resonance is a function of both the beam length and diameter. Based on this observation, we propose here a passive spatial multiplexer with a clear understanding of the physics, controlling the two types of beam resonances with independent geometrical parameters, i.e. length and diameter. It has the potential for mechanical filtering A0 Lamb wave in a narrow frequency band, over a wide range of frequencies. Numerical simulations show that the multiplexer waveguides that result have negative refraction indices. Finally, we show that the geometrical periodicity inside of the multiplexing line strongly influences the efficiency of the transmission through the waveguide, highlighting a Fano + Bragg scattering in play.

Theoretical approach

Starting with the fully elastic formulation from Colquitt et al. [19], we estimate the consequences of changing the resonators diameter on the main bandgap and on the narrow flexural leakage independently. Results of this analysis are presented in Fig. 2b, in a restricted frequency band including the end of the passband (~5 kHz) and the targeted leakage frequency interval (~6 kHz). The main bandgap induced by the compressional motion is highlighted by the red background color. The flexural resonances create three distinct narrow bands that leak inside the bandgap, depending on the beam diameter, as highlighted with the dotted square in Figure 2b. Changing the resonators diameter thus has a significant impact on the leakage through the flexural resonance, without affecting the main bandgap.

These results are used here to build a multiplexer by introduction of local defects into the metamaterial waveguide. These defects are obtained by changing the beam diameter for one line of beams, hence by de-tuning their flexural resonances. In practice, each resonance, either longitudinal or flexural, results in a phase jump at the bottom of the beams. The longitudinal resonance is associated to the up-and-down beam motion that induces a negative apparent density as seen by the plate [Williams et al. 2015, Lott et al. 2019] with a monopolar radiation into the plate. Similarly, the flexural resonance induces a bending momentum at the bottom of the beams and thus a dipolar radiation into the plate. The resulting A_0 scattered field differs substantially depending on the resonators motion.

The tuned leakage through the metamaterial region represents the association of monopole and dipole resonances, which is crucial to obtain double-negative materials, as is demonstrated herein. In the perspective of further experimental realization with this device, the geometry constrain here may require a 3D printing technic to create the sample, with a resolution on the geometry construction less than 0.1 mm.

Numerical simulations

We used the COMSOL simulation software to study the propagation of the antisymmetric A_0 Lamb mode into a metasurface made of 11 × 21 regularly spaced beams. The simulation box is depicted in Figure 2a, which includes the beam cluster (Fig. 2a-1) and the absorbing areas (Fig. 2a-2). The source is a plane wave (Fig. 2a-3) that is emitted from the right side of the metasurface region and transmitted through the beam cluster.

For the propagating simulations, the system is discretized using two-dimensional (2D) shell elements to model the plate, and 1D beam elements for the resonators, both of which are available in the structural dynamic toolbox of COMSOL. This strategy greatly decreases the model complexity and the computing time, while preserving the full physics of the system. Using a 2-mm thick plate in the numerical scheme, both A_0 and S_0 are reproduced from 0 kHz to 10 kHz, along with the compressional and flexural motion of the beam. We use the same material and geometry as defined in Figure 3c. It is now straightforward to introduce local changes in the beam diameter (Fig. 1c), the key parameter in this study, without worrying about meshing instabilities that would arise using full 3D finite elements.

The absorbing boundaries are designed using the approach described in [21], with eight different areas that surround the model zone representing the space-dependent attenuation (which increases exponentially from the boundary of the propagating zone to the end of the simulation box). Finally, the full computation takes approximatively one hour in the frequency domain (around 45 seconds per frequency). This strategy provides a high frequency resolution in a narrow bandwidth, with limited numerical cost.

Qualitative and quantitative results

We ran three different simulations with varying diameters for the central line of the beam cluster (i.e., the waveguide). The background metamaterial consists of beams with a diameter of 5.5 mm and a length of 61 cm. The central line diameters are 5.2 mm, 5.3 mm, and 5.4 mm for the three simulations. Figure 3 shows the qualitative results of the transmitted intensities here. In the frequency band of 6.0 kHz to 6.3 kHz (subpanels 1 to 3 in Figure 3), each selected diameter (subpanels a to c in Fig. 3) creates a leakage at a very precise frequency, thus realizing a frequency-based selector for the A_0 Lamb mode.

We also compute the apparent transmission coefficient, as well as the effective wavenumber inside this waveguide. Figure 4 shows the overall results for the normalized transmitted coefficient (Fig. 4a) and the effective wavenumber (Fig. 4b). In Figure 4a, the three simulations are normalized by the maximum transmitted intensity in the 6.00 kHz to 6.35 kHz band. At around 6.40 kHz (not shown here), the background array made with 5.5-mm-diameter beams globally resonated, which breaks up the wave guidance along the central line. Below this frequency, the three colors in Fig. 4a (blue, red, black) that correspond to the three above-mentioned central line diameters highlight three separate transmission peaks.

For the wavenumber, we simply determine the wave speed along the waveguide. We select three regions to compute the effective wavenumber around each of the transmitted peaks of the three simulations, as plotted in Figure 4b in a $\mathrm{f}-\mathrm{k}$ frequency-wavenumber graph. We compute the spatial Fourier transform of the wavefield along the line, and select the propagative wavenumber in the positive y-direction.

The negative slope of the phase speed with respect to frequency can be noted here. With a negative slope in the f-k graph, and thus a negative group velocity, the double negativity typical response of this metamaterial is highlighted. Due to the periodicity of the designed array, we display the calculation of the effective wavenumber on the Brillouin edges ($\Gamma-\mathrm{X}$) (Fig. 4b). However, we do not observe any spectral folding after $'\mathrm{X}'$ here. Note that the $\Gamma-\mathrm{X}$ direction (Fig. 4b) corresponds to the the reciprocal space ‘y’ direction in Figure 2c.

Also, along with these three detected bands, we compute the spatial–spectral amplitude of the tangential and normal components of the wavefield that propagates along the positive y-direction, for the previously estimated wavenumber. We estimate the horizontal versus vertical motion of the plate through the spatial Fourier transform of both in-plan (h) and out of plane (v) motion of the plate surface. The obtained values are reported in color scale in Fig. 4b.With the ratio u/v (i.e., the tangential vs vertical components), we observe smooth transition between 'quasi' tangential waves and 'quasi' normal ones. This transition was already expected by Rupin et al. [22], who also described the coupling between the two orthogonal Lamb modes of the free plate (A_0-S_0) in this frequency regime.

Discussion

Previous analytical studies of such a plate+beam system have highlighted the dependency between the slope of the quasi-flat band induced by the flexural resonance inside the bandgap and the overall geometric properties of the system. In particular, the thickness of the plate substrate [19] influences the emergence of a negative index transmission band. Indeed, if the plate is thin enough, the bending moment induced by the flexural resonance of the beams can add negative mass density, in addition to the negative Young's modulus induced by the longitudinal resonance inside the bandgap [Williams et al. 2016], and thus yield a negative group velocity [23].

In practical instances, double-negative materials come with high attenuation effects [10]. Here, due to the finite size of the system, our transmission coefficient calculation does not capture quantitatively the reflection magnitude at the plate/metamaterial interface. However, previous experimental and numerical data have demonstrated that leakage of such a flexural resonance inside the wide bandgap induced by the compressional motion of the beams can be easily detected [22, 24]. In the present study, we move our attention to the propagation mechanism along the defect line through the introduction of progressive disorder in the multiplexer geometry, to thus identify the scattering regime in play. The results of such simulations are shown in Figure 4.

The numerical model is similar to that shown in Figure 3b. The disorder is implemented by induction of a small spatial random variation along the waveguide (0-6 mm, drawing from a uniform distribution). For each disorder value, three simulations were run, with calculation of the mean transmitted intensity spectra. The results of these spectra are shown in Figure 5a. With disorder, the transmission peak decreases in amplitude. The mean transmitted intensity integrated on the full frequency band (6160-6240 Hz) is shown in Figure 5b as a function of the disorder, where the error bars represent the standard deviations of the simulation results for each disorder value. It is worth noting that the fluctuations over disorder are stronger at a single frequency than in the integrated frequency band.

Figure 5c-e (Fig. 5c is the same as Fig. 3b, but at 6195 Hz) shows the intensity map at 6195Hz for three particular values of the disorder (i.e., 0, 2, 5 mm random displacement of the beams). In Figure 5c, the beams are depicted as small circles with a black-to-white color scale as the logarithm of the beam motion intensity, and a green-to-yellow color scale as the normalized transmitted intensity (the norm is the maximal transmitted intensity with 0 disorder, as in Fig. 3). We observe that with increasing disorder, the intensity diffusion across the central line might stop. This result differs from previous experimental studies showing the non-effect of the randomness of the beams positions on the main A0 passband [16]. Here, the spatial ordering is essential in this propagative branch, making the coupling between S0 and A0 Lamb mode possible, from the tangential force in the low spatial frequency regime (low-k values), to the predominance of the bending motion in the high spatial frequencies (high-k values). We conclude that the propagation in this frequency band is due to Bragg dipolar scattering between successive aligned beams, which is highly sensitive to disorder. In the absence of disorder, the combination met the criteria for a one dimensional negative index material, resulting in the negative slope in the f-k representation of Figure 4b.

Conclusion

We demonstrate here the possibility to model a device that can filter and guide low-frequency Lamb waves in a thin plate using the modal overlap of the flexural and compressional resonances of the beam-like resonators. The frequency position of the flexural resonance where the leakage is observed can be adjusted by acting on the diameter of one line of beams, which does not affect the longitudinal resonance that controls the main bandgap. Building on these results, we model a mechanical wave multiplexer that can select the narrow frequency flexural Lamb mode inside a wide frequency bandgap.

With the combination of two scattering modes, one monopolar and one dipolar, the resulting effective material has a negative refraction index with fast evolution of wave polarization over frequency. The effects of the randomness of the beam positions on the waveguide efficiency are also evaluated, and these confirm the predominance of a Bragg scattering mechanism of intensity diffusion for the flexural resonance of the beams, in addition to the mechanical constraints at the beam attachment due to compressional resonance inside the main bandgap. These results highlight the strong interplay between hybridization due to local resonance, hybridization between different resonant modes, and Bragg scattering versus incoherent scattering. We believe these results can be adapted to any locally resonant system if the individual resonators overlap in their Fano resonances.

References

[1] Pendry, J. B. (2000). Negative refraction makes a perfect lens. Physical Review Letters, 85(18), 3966.

[2] Page, J. H. (2016). Focusing of ultrasonic waves by negative refraction in phononic crystals. AIP Advances, 6(12), 121606.

[3] Colombi, A., Craster, R. V., Colquitt, D., Achaoui, Y., Guenneau, S., Roux, P., & Rupin, M. (2017). Elastic wave control beyond band-gaps: shaping the flow of waves in plates and half-spaces with sub-wavelength resonant rods. Frontiers in Mechanical Engineering, 3, 10.

[4] Savo, S., Casse, B. D. F., Lu, W., & Sridhar, S. (2011). Observation of slow-light in a metamaterials waveguide at microwave frequencies. Applied Physics Letters, 98(17), 171907.

[5] Zhu, R., Chen, Y. Y., Wang, Y. S., Hu, G. K., & Huang, G. L. (2016). A single-phase elastic hyperbolic metamaterial with anisotropic mass density. The Journal of the Acoustical Society of America, 139(6), 3303-3310.

[6] Chen, Y., Hu, J., & Huang, G. (2016). A design of active elastic metamaterials for control of flexural waves using the transformation method. Journal of Intelligent Material Systems and Structures, 27(10), 1337-1347.

[7] Yves, S., Berthelot, T., Fink, M., Lerosey, G., & Lemoult, F. (2019). Left-handed band in an electromagnetic metamaterial induced by sub-wavelength multiple scattering. Applied Physics Letters, 114(11), 111101.

[8] Shang, X., Wang, Y., Xia, W., & Lancaster, M. J. (2013). Novel multiplexer topologies based on all-resonator structures. IEEE Transactions on Microwave Theory and Techniques, 61(11), 3838-3845.

[9] Wang, W., Bonello, B., Djafari-Rouhani, B., Pennec, Y., & Zhao, J. (2018). Double-negative pillared elastic metamaterial. Physical Review Applied, 10(6), 064011.

[10] Brunet, T., Merlin, A., Mascaro, B., Zimny, K., Leng, J., Poncelet, O., ... & Mondain-Monval, O. (2015). Soft 3D acoustic metamaterial with negative index. Nature Materials, 14(4), 384.

[11] Yves, S., Lemoult, F., Fink, M., & Lerosey, G. (2017). Crystalline soda can metamaterial exhibiting graphene-like dispersion at sub-wavelength scale. Scientific Reports, 7(1), 15359.

[12] Miniaci, M., Pal, R. K., Morvan, B., & Ruzzene, M. (2018). Experimental observation of topologically protected helical edge modes in patterned elastic plates. Physical Review X, 8(3), 031074

[13] Miniaci, M., Gliozzi, A. S., Morvan, B., Krushynska, A., Bosia, F., Scalerandi, M., & Pugno, N. M. (2017). Proof of concept for an ultrasensitive technique to detect and localize sources of elastic nonlinearity using phononic crystals. Physical Review Letters, 118(21), 214301.

[14] Tokushima, M., Kosaka, H., Tomita, A., & Yamada, H. (2000). Lightwave propagation through a 120 sharply bent single-line-defect photonic crystal waveguide. Applied Physics Letters, 76(8), 952-954.

[15] Benchabane, S., Gaiffe, O., Salut, R., Ulliac, G., Laude, V., & Kokkonen, K. (2015). Guidance of surface waves in a micron-scale phononic crystal line-defect waveguide. Applied Physics Letters, 106(8), 081903.

[16] Rupin, M., Lemoult, F., Lerosey, G., & Roux, P. (2014). Experimental demonstration of ordered and disordered multiresonant metamaterials for Lamb waves. Physical Review Letters, 112(23), 234301.

[17] Williams, E. G., Roux, P., Rupin, M., & Kuperman, W. A. (2015). Theory of multiresonant metamaterials for A_0 Lamb waves. Physical Review B, 91(10), 104307.

[18] Lott, M., & Roux, P. (2019b). Locally resonant metamaterials for plate waves: the respective role of compressional versus flexural resonances of a dense forest of vertical rods. Fundamentals and Applications of Acoustic Metamaterials: From Seismic to Radio Frequency, 1, 25-45.

[19] Colquitt, D. J., Colombi, A., Craster, R. V., Roux, P., & Guenneau, S. R. L. (2017). Seismic metasurfaces: Sub-wavelength resonators and Rayleigh wave interaction. Journal of the Mechanics and Physics of Solids, 99, 379-393

[20] Lott, M., & Roux, P. (2019). Effective impedance of a locally resonant metasurface. Physical Review Materials, 3(6), 065202.

[21] Morvaridi, M., & Brun, M. (2018). Perfectly matched layers for flexural waves in Kirchhof–Love plates. International Journal of Solids and Structures, 134, 293-303.

[22] Rupin, M., Roux, P., Lerosey, G., & Lemoult, F. (2015). Symmetry issues in the hybridization of multi-mode waves with resonators: an example with Lamb waves metamaterial. Scientific Reports, 5, 13714.

[24] Lott, M., Roux, P., Seydoux, L., Tallon, B., Pelat, A., Skipetrov, S., & Colombi, A. (2020). Localized modes on a metasurface through multiwave interactions. Physical Review Materials, 4(6), 065203.

[23] Wu, Y., Lai, Y., & Zhang, Z. Q. (2007). Effective medium theory for elastic metamaterials in two dimensions. Physical Review B, 76(20), 205313.

Figures

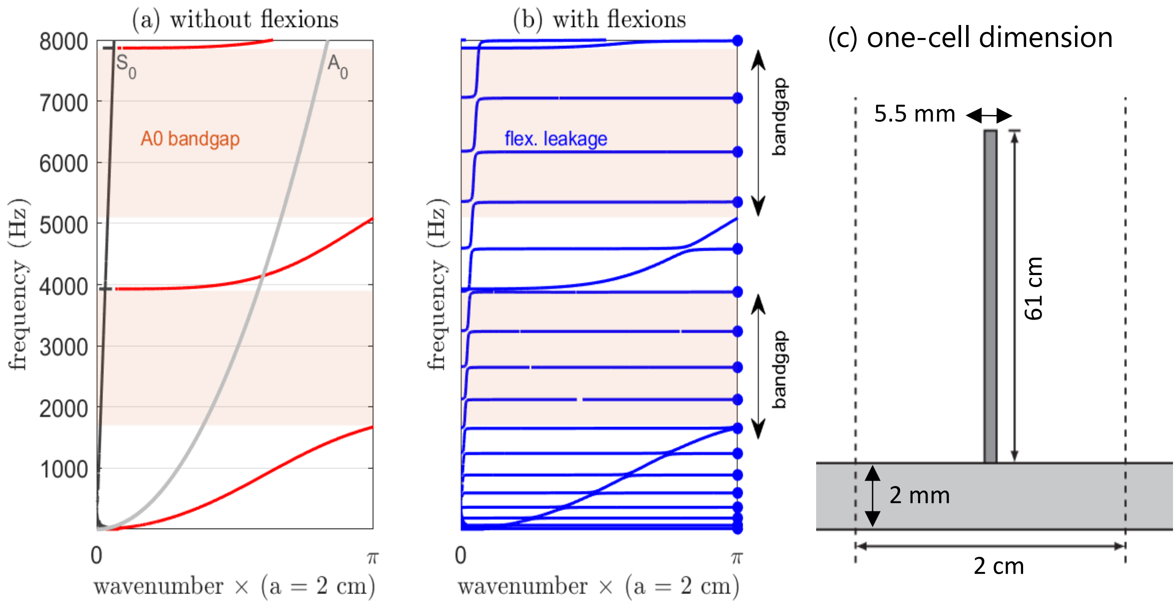

Figure 1: Theoretical dispersion relation for an infinite array of beams [Colquitt 2016]. (a) Dispersion curves obtained neglecting the beam's flexural resonance effects. (b) Dispersion curves with the flexural resonance effects. (c) Cell dimensions and properties: Lattice constant a = 2 cm, beam length L = 0.61 m, beam diameter db = 5.5 mm, plate stiffness h = 2 mm and, aluminum for the material (E = 69 GPa, nu = 0.33).

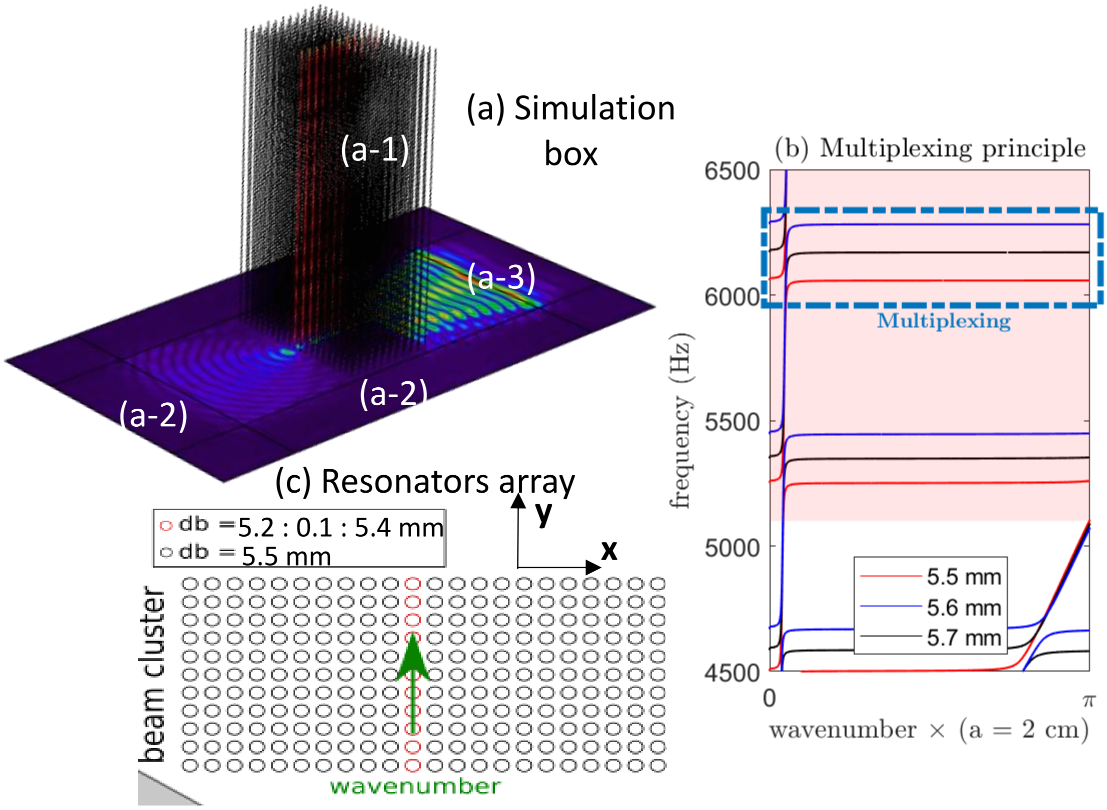

Figure 2: Simulation procedure. (a) The metamaterial (a-1) is made of 11 × 21 regularly spaced beams attached on a 2-mm-thick plate surrounded by absorbing areas (a-2). A plane wave (a-3) is emitted from the right side of the beam cluster. (b) Typical band structure for three beam diameters. Inside the bandgap (redish background area), each flexural resonance creates a different narrow leakage (dashed rectangle area). (c) Using a different beam diameter along a central line inside the beam cluster tunes the flexural resonance position without affecting the beginning of the bandgap in this region.

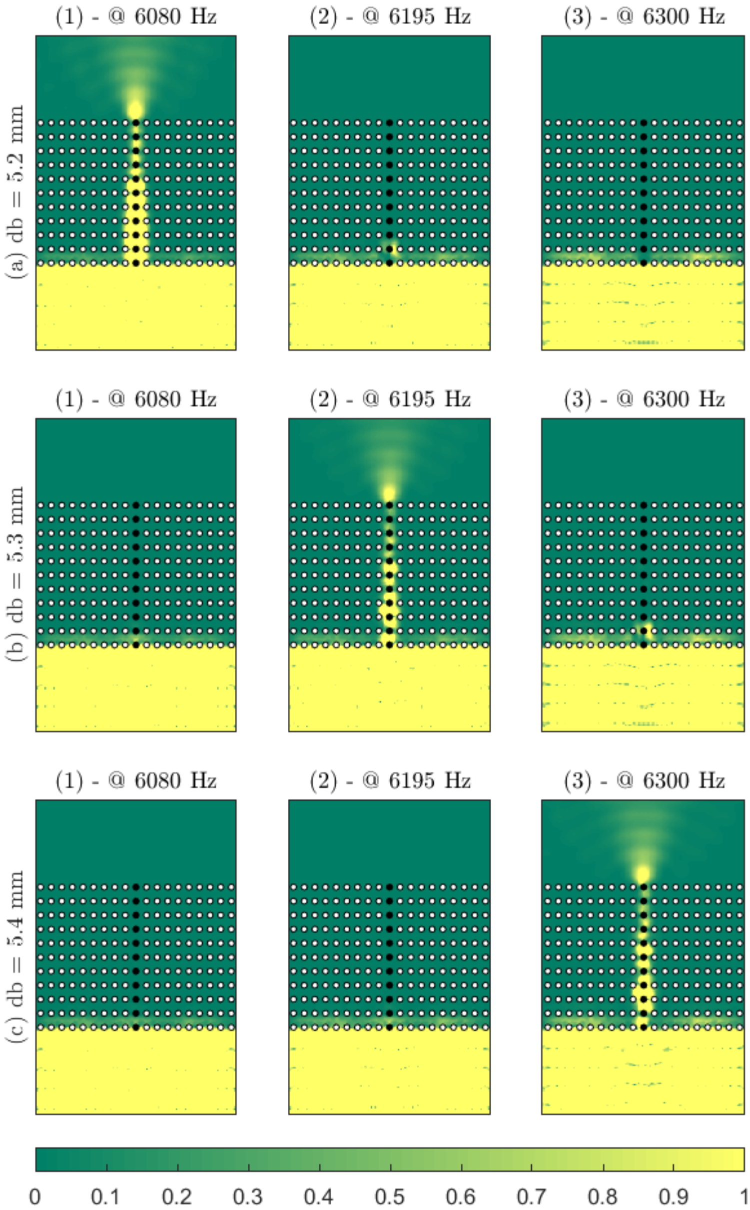

Figure 3: Normalized intensity maps for the three-designed waveguides (normalized by maximum transmitted intensity for each simulation box). The white points represent the 5.5-mm-diameter beams of the cluster, and the black points indicate the 5.2 mm (a), the 5.3 mm (b), and the 5.4 mm (c) diameter beams of the central line. From top to bottom (a-c): increasing the beam diameter of the central line increases the frequency of the flexural resonance and tunes the leakage through the beam cluster.

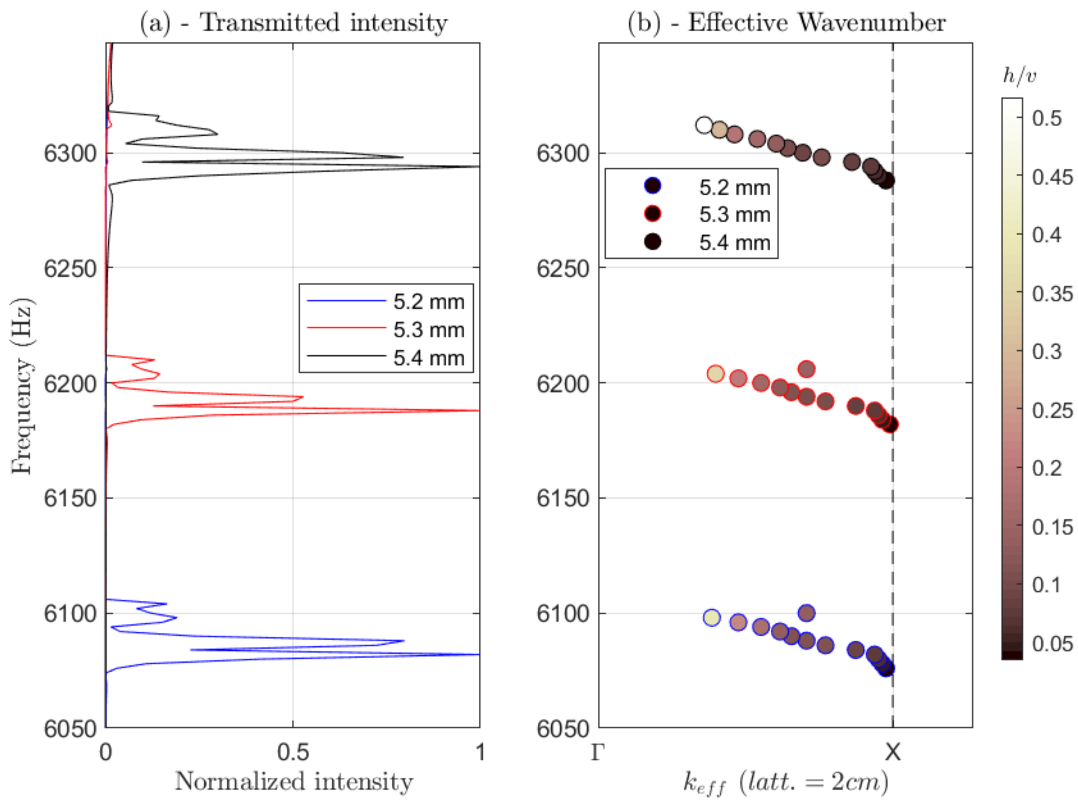

Figure 4: (a) Normalized transmission coefficients for the three simulations (blue, red, black) that create three different leakages. (b) Band structure of the created waveguides (blue, red, black circles). The color scale in (b) depicts the wave polarization through the u/v ratio (i.e., tangential vs normal components), computed from the spatial Fourier transform.

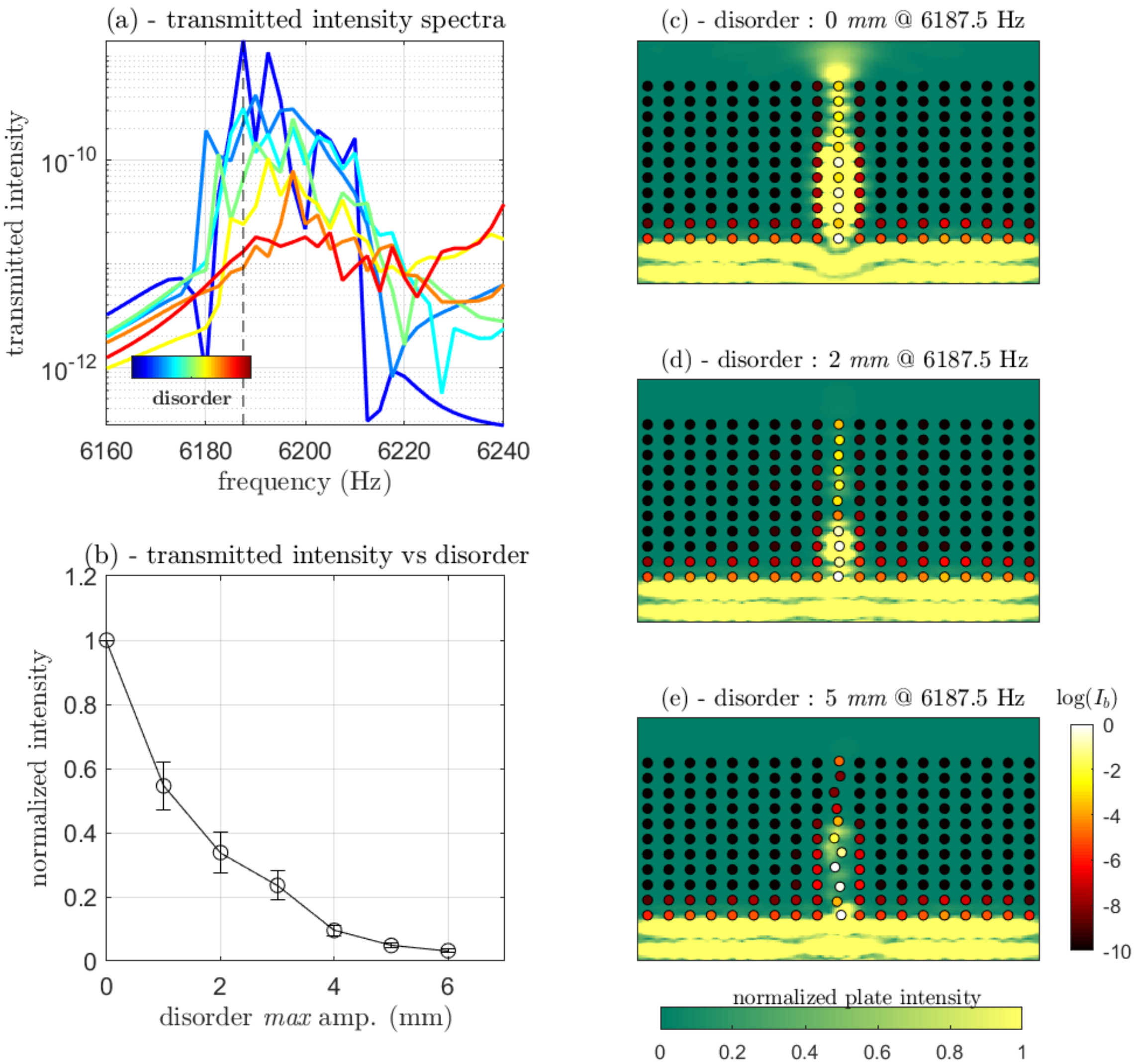

Figure 5: Effects of the randomness of the central line beam positions on the transmission intensity. (a) Mean transmission spectra for the 5.3-mm-diameter beams in the central line and the different values of the disorder. (b) Normalized transmitted intensity versus amplitude of the disorder, as indicated. (c) same as Figure 2b at 6195Hz. (d, e) Intensity map at 6195 Hz for 2 mm and 5 mm random displacements of the beams in the central line. The intensity maps are normalized by the maximum transmitted intensity for the case without disorder. (c-e) The beam motion amplitude is depicted as a ‘log’ scale.